Supporting Information

Beilharz et al. 10.1073/pnas.1119172109

SI Materials and Methods

Strains, Plasmids, and Growth Conditions. *Streptococcus pneumoniae* strains R6 and D39 were grown at 30 °C or 37 °C in C+Y medium (1) or in GM17 medium (2). Blood agar plates were made from Columbia agar containing 3% defibrinated sheep blood (Johnny Rottier, Kloosterzade, The Netherlands). For induction of P_{czcD} (hereafter, P_{Zn}), $ZnSO_4$ or $ZnCl_2$ was added to liquid medium and blood agar plates. Competent *S. pneumoniae* R6, D39, and Rx1 cells were prepared as described previously by the addition of competence-inducing peptide CSP-1 (1).

Recombinant DNA Techniques and Oligonucleotides. Common DNA procedures such as DNA isolation, restriction, ligation, gel electrophoresis, and transformation of *Escherichia coli* were performed as described (3). Chromosomal DNA of *S. pneumoniae* was isolated using the Promega Wizard Genomic DNA Purification Kit. Oligonucleotides used in this study are listed in Table S2 and were purchased from Biolegio or Metabion. Enzymes were purchased from Roche, New England Biolabs, Bioline, and Fermentas and were used as described by the manufacturer. For PCR amplification, Velocity polymerase (Bioline) or Pfu polymerase (Stratagene) was used.

Western Blot Analysis and Immunodetection. Cells were grown in C+Y medium (4 mL) with the addition of $ZnSO_4$ to a final concentration of 0.15 mM and at an OD_{600} ~0.3 and were harvested by centrifugation at 9,000 rpm (Eppendorf tabletop centrifuge) for 5 min. For lysis, the pellet was resuspended in 100 μL of SDS, EDTA, deoxycholate, salt (NaCl); 0.02%/15 mM/0.01%/150 mM) (SEDS) lysis buffer and was incubated for 5 min at 37 °C. Lysates were diluted in 100 μL 2× SDS loading buffer and boiled for 5 min. After separation by SDS/PAGE, proteins were transferred to a PVDF membrane by Western blotting. GFP fusion proteins were detected with polyclonal anti-GFP antibodies (Invitrogen) and HRP-conjugated anti-rabbit IgG antibody (GE Healthcare) according to the manufacturer's instructions. StkP, PhpP, and DivIVA were detected using custom-made polyclonal rabbit anti-StkP, anti-PhpP, and anti-DivIVA antibodies.

In Vitro Protein Phosphorylation of FtsA Mutant Proteins. Recombinant substrate protein (0.4 μg) was phosphorylated in the presence of 0.4 μg of purified StkP kinase domain (StkP-KD) in kinase buffer containing 25 mM Tris·HCl (pH 7.5), 25 mM NaCl, 5 mM $MnCl_2$, 10 μM ATP, and 1 μCi γ[^{32}P]ATP. The reaction was started by the addition of ATP and was terminated after 15 min of incubation in 37 °C by the addition of 5× SDS sample buffer. Samples were separated by SDS/PAGE, and the Coomassie blue-stained gel was exposed to a sensitive screen and scanned with Molecular Imager FX (Bio-Rad).

Construction of Plasmids and Strains. ***Construction of pJWV25-based plasmids and strains.*** To construct the plasmid pJWV25-StkP, carrying the *gfp*$^+$ variant fused to the *S. pneumoniae stkP* gene under the control of the zinc-inducible P_{czcD} promoter (P_{Zn}), a PCR was performed using the primers stkP-F+SpeI and stkP-R+NotI and chromosomal DNA from *S. pneumoniae* D39 as a template. The PCR products subsequently were cleaved with NotI and SpeI and ligated into the corresponding sites of pJWV25 (4), resulting in the plasmid pJWV25-StkP. Plasmids pJWV25-PhpP, pJWV25-kinase, pJWV25-TM-kinase, pJWV25-PASTA, and pJWV25-FtsA were constructed in a similar manner but using the primer pairs phpP-F+SpeI and phpP-R+NotI, stkP-F+SpeI and stkP-kinase-R+NotI, stkP-F+SpeI and stkP-TM-R+NotI, stkP-PASTA-F+SpeI and stkP-R+NotI, and FtsA-F+SpeI and FtsA-R+NotI, respectively. To construct plasmid pJWV25-GFP-StkP-K42R, StkP-K42R was amplified using the primer pair stkP-F+NotI and stkP-R+SpeI and pEX-StkP-K42R (5). The PCR products were cleaved with NotI and SpeI and ligated into the corresponding sites of pJWV25 (4).

To construct plasmid pJWV25-DivIVA-GFP, we performed fusion PCR to fuse P_{Zn}, *divIVA*, and *gfp*$^+$ separated from *divIVA* via a flexible hinge region. P_{Zn} was amplified using primers LN123 and LN133 with pJWV25 (4) as a template. The *divIVA* gene was amplified with primers LN131 and LN181 with *S. pneumoniae* Rx1 chromosomal DNA as a template. PCR products corresponding to P_{Zn} and *divIVA* were used as templates in a fusion PCR with primers LN123 and LN181. In the next step, we amplified the *gfp*$^+$ gene using primers LN180 and LN179 with plasmid pJWV25 as a template. Primer LN179 was designed to contain a hinge region to separate the GFP and DivIVA moieties of the fusion protein flexibly. Fusion products P_{Zn}-*divIVA* and *gfp*$^+$ were used as templates in another fusion PCR using primers LN123 and LN180. The resulting PCR product, coding for the P_{Zn}-*divIVA-gfp*$^+$ sequence, was digested with EcoRI and NotI and was ligated in the corresponding sites of pJWV25, resulting in pJWV25-DivIVA-GFP.

To construct pJWV25-stkP′-prkC′, the kinase domain of StkP [1,095 bp; amino acids 2–365 (w/o ATG/Met)] was amplified with primers LN144 and LN145 using *S. pneumoniae* Rx1 chromosomal DNA as template. The sequence coding for the C-terminal part of PrkC containing its predicted PASTA repeats [879 bp (including TAA), amino acids 357–648] was amplified with primers LN146 and LN147 using chromosomal DNA of *Bacillus subtilis* as a template. The two resulting amplicons were used as a template in a fusion PCR using primers LN144 and LN147. The subsequent *stkP-prkC* fusion fragment was digested with SpeI and NotI and cloned in the corresponding sites of vector pJWV25 (4).

Strains KB02-20, KB02-23, KB02-60, KB02-62, KB02-63, HK95, and HK96 were obtained by a double-crossover recombination event between the chromosomal *bgaA* gene of strain R6 and the *bgaA* regions located on plasmids pJWV25-StkP, pJWV25-PhpP, pJWV25-StkP′-PrkC′, pJWV25-FtsA, pJWV25-DivIVA-GFP, pJWV25-FtsA-RFP-StkP, and pJWV25-DivIVA-GFP-RFP-StkP, respectively. Strains KB01-15, KB01-14, JWV403, KB01-40, and KB01-16 were obtained by a double-crossover recombination event between the chromosomal *bgaA* gene of strain D39 and the *bgaA* regions located on plasmids pJWV25-StkP, pJWV25-PhpP, pJWV25-kinase, pJWV25-TM-kinase, and pJWV25-PASTA, respectively. Strain KB02-61 was obtained by a double-crossover recombination event between the chromosomal *bgaA* gene of strain KB02-29 and the *bgaA* regions located on plasmid pJWV25-StkP′-PrkC′. For transformation of *S. pneumoniae*, 2 μL of plasmid DNA (~200 ng) was added to competent cells followed by a phenotypic expression period of 90 min at 37 °C and overnight growth on Columbia blood agar plates containing tetracycline (1 μg/mL). Transformants were restreaked to single colonies, and correct integration into the *bgaA* locus was verified by PCR.

S. pneumoniae strains KB02-64, KB01-18, KB02-65, and KB02-29 were obtained by transformation of strains KB02-63, KB01-15, KB02-62, and R6, respectively, with chromosomal DNA of strain Sp10 (6). Strains KB02-22, KB01-20, and KB01-21 were obtained by transformation of strains KB02-20, KB01-15, and KB01-14,

respectively, with plasmid pDEL*phpP-stkP*. Transformants were selected on Columbia blood agar plates containing 4.5 μg/mL chloramphenicol after overnight incubation at 37 °C. Strain KB01-19 (P_{Zn}-*gfp-phpP*, Δ*phpP*) was constructed by transforming strain KB01-14 with plasmid pDEL*phpP*. Strain KB02-66 was obtained by transforming strain KB02-23 with plasmid pDELstkP. Transformants were selected on Columbia blood agar plates containing 4.5 μg/mL chloramphenicol and 0.1 mM $ZnSO_4$ after overnight incubation at 37 °C. We note that Δ*phpP* transformants were obtained using highly competent cells but at a significantly lower frequency (>10-fold less) compared with the generation of *stkP* mutants. Furthermore, Western blot analyses indicate a possible polar effect of the *phpP* mutation on StkP expression. Therefore, we cannot comment on the potential essentiality of *phpP* as suggested previously (6).

Strains KB02-26, KB02-27, and KB02-28 were obtained by a double-crossover recombination event between the chromosomal *bgaA* gene of strain R6 and the *bgaA* regions located on plasmids pJWV25-kinase, pJWV25-PASTA, and pJWV25-TM-kinase, respectively. Strains KB02-79 (P_{Zn}-*gfp-kinase*, Δ*stkP*), KB02-81 (P_{Zn}-*gfp-TM-PASTA*$_{1–4}$, Δ*stkP*), KB02-80 (P_{Zn}-*gfp-kinase-TM*, Δ*stkP*), and KB02-78 (P_{Zn}-*gfp-stkP-K42R*, Δ*stkP*) were obtained by transforming strains KB02-26, KB02-27, KB02-28, and KB02-77, respectively, with pDEL*stkP* (5).

Strain KB02-34 (P_{Zn}-*gfp-stkP;* Δ*divIVA*) was obtained by transformation of strain KB02-20 with chromosomal DNA of Δ*divIVA* strain (7).

Strains Sp31 (P_{Zn}-*gfp-phpP*; Rx1) and Sp79 (P_{Zn}-*gfp-phpP*; *stkP-K42R;* Rx1) were obtained by transformation of wild-type Rx1 and Sp19 (*stkPK42R*; Rx1) (5), respectively, with pJWV25-PhpP. Strain Sp32 (P_{Zn}-*gfp-stkP*; Rx1) was constructed by transformation of wild-type Rx1 with pJWV25-StkP.

FtsA overproduction plasmids. To construct plasmid pETPhos-1511, a PCR using primers LN182 and LN183 was performed with *S. pneumoniae* Rx1 chromosomal DNA as a template. The amplified fragment subsequently was cleaved with NdeI and XhoI and ligated in the corresponding sites of plasmid pETPhos (8). To introduce phosphoablative mutations in the *ftsA* gene in plasmid pETPhos-1511, we used the QuikChange mutagenesis kit (Stratagene) and mutagenic oligonucleotides in the following combinations: LN186 and LN187 for mutation T116A; LN188 and LN189 for mutation T160A; and LN190 and LN191 for mutation S113A.

Construction of* S. pneumoniae *ΔphpP and ΔphpP-stkP mutants. Deletion of the *phpP* and *phpP-stkP* genes was achieved by transformation of *S. pneumoniae* wild-type strain with a vectorless DNA fragment consisting of *phpP* or *phpP-stkP* downstream and upstream regions of homology and a *cat* cassette replacing the *phpP* or *phpP-stkP* coding region, as described by Nováková et al. (5). Briefly, the *phpP* upstream flanking region (800 bp) was amplified with primers UFPFP and UFPRP. The downstream flanking region of phpP (760 bp) was amplified with primers DFPFP and DFPRP, and primers CAT1 and CAT2 were used to amplify the terminatorless *cat* gene from plasmid pEVP3 (9). The downstream flanking region of *stkP* (820 bp) was amplified with primers DFKFP and DFKRP, and primers CAT1 and CAT3 were used to amplify the terminatorless *cat* gene from plasmid pEVP3. The final constructs pDELphpP and pDELphpP-stkP were prepared by subsequent directional cloning of the fragments into Bluescript vector (5′ region-*cat* gene-3′ region) using restriction sites included in the primers. The resulting chloramphenicol-resistant clones arising from the double-crossover event were examined for successful allelic exchange by diagnostic PCR and Southern hybridization. The junctions between exogenous and chromosomal DNA in allelic exchange mutants were verified by sequencing.

Construction of strain Sp38. To introduce an extra copy of the *stkP* gene under the inducible promoter into the dispensable *bgaA* locus on the *S. pneumoniae* chromosome, we constructed plasmid pZn-StkP. First, *stkP* was amplified with primers LN121 and LN134 with Rx1 chromosomal DNA as a template. The P_{Zn} promoter was amplified with primers LN123 and LN120 from template plasmid pJWV25 (4). Both PCR products were used as a template in a fusion PCR with primers LN123 and LN134. The final PCR product coding for *stkP* fused with P_{Zn} was digested and cloned into the EcoRI and NotI restriction sites of plasmid pJVW25. *S. pneumoniae* wild-type strain Rx1 was transformed with PvuI-digested pZn-StkP plasmid. The tetracycline-resistant transformants were examined for successful allelic exchange using diagnostic PCR, and the resulting strain was named "Sp32." To delete the native *stkP* gene, we transformed strain Sp32 with SacII-digested pDELstkP plasmid, as described previously (5), resulting in the strain named "Sp38" (Δ*stkP*, *bgaA*::P_{Zn}-*stkP*).

Fluorescence Microscopy. Cells were grown at 37 °C in C+Y or GM17 medium in half-filled 5-mL capped tubes to allow enough aeration for proper GFP maturation. Then 0.5 mL of cell culture was spun down, and the pellet was washed with 150 μL PBS, as described (10). Where relevant, Nile red (Invitrogen) was added to a final concentration of 8 ng/mL. Then 0.4 μL of the cell suspension was spotted on a microscope slide containing a slab of 1% PBS agarose. Images were taken with a Deltavision (Applied Precision) IX71Microscope (Olympus) using a CoolSNAP HQ2 camera (Princeton Instruments) with a 100× phase-contrast objective. Emission/excitation filters were from Chroma. For GFP, typical exposure times were between 0.8 and 1.5 s with 100% xenon light (300 W). For Nile red, typical exposure times were 200 ms with 32% of excitation light. Microscopy images were deconvolved using softWoRx 3.6.0 (Applied Precision) and modified for publication using ImageJ (http://rsb.info.nih.gov/ij/) and CorelDRAW ×3 (Corel Corporation). Phase-contrast images were segmented automatically and analyzed using Microbetracker (11), and cell-length distributions were plotted using MATLAB 7.10.

Immunofluorescence Microscopy. Immunofluorescence experiments were carried out as previously described (12). Briefly, strains Rx1 and Sp38 (Rx1, Δ*stkP*, P_{Zn}-*stkP*) were grown exponentially in Tryptic Soy Broth (Oxoid) medium in the absence of zinc, washed three times in 10 mM phosphate (pH 7.0), and fixed for 15 min at room temperature and for 45 min on ice in 4% (wt/vol) paraformaldehyde (Immunofix; Bio-Optica). Cells then were transferred onto SuperFrost Plus slides (Menzel-Glaser). The slides were washed twice with PBS, air dried, dipped in methanol at −20 °C for 10 min, and allowed to dry. After rehydration with PBS, the slides were blocked for 1 h at room temperature with 2% (wt/vol) BSA and 0.2% Triton X-100 (vol/vol) in PBS (BSA-PBST) and for 1 h with appropriate dilutions of anti-DivIVA antibodies in BSA-PBST. The slides then were washed five times with PBST and incubated for 30 min with a 1:500 dilution of anti-rabbit Ig (IgG) Alexa Fluor 488 (Invitrogen). Finally, preparations were stained with a fluorescence antifade solution containing propidium iodide (0.5 μg/mL) and 2% (wt/vol) 1,4-diazabicyclo[2.2.2] octane (DABCO), all obtained from Sigma. Slides were observed using a Zeiss Axioplan 2 equipped with a 100× Achroplan fluorescence objective and standard filter sets (Zeiss no. 09, no. 15, and no. 24). Photographs were taken with a Canon Powershot G6 digital camera, acquired with a Canon Zoom Browser, and processed with Adobe Photoshop 6.0.

Fluorescently Labeled Vancomycin Microscopy. Fluorescently labeled vancomycin (Van-FL) staining was performed as recently described (13). Briefly, strains Rx1 or Sp38 (Rx1, Δ*stkP*, P_{Zn}-*stkP*) were grown exponentially in the absence of zinc. Samples were collected and incubated with 2 μg/mL Van-FL (Molecular Probes) for 20 min at 37 °C. Cells were centrifuged, washed three

times with PBS, and fixed in paraformaldehyde 4% (wt/vol) (Immunofix; Bio-Optica). Cells then were spotted on glass slides, air dried, washed with PBS, mounted with DABCO, and observed using a Zeiss Axioplan 2 equipped with a 100× Achroplan fluorescence objective. Photographs were taken with a Canon Powershot G6 digital camera, acquired with a Canon Zoom Browser, and processed with Adobe Photoshop 6.0.

Van-FL staining on unfixed cells was performed basically as described previously (14). Wild-type R6 and KB02-29 (R6, Δ*stkP*) strains were grown to OD_{600} 0.15. Samples were labeled with 0.2 μg/mL of Van-FL/vancomycin (50:50 mixture) (kind gift of D. J. Scheffers, Molecular Microbiology, University of Groningen, the Netherlands) for 5 min before examination by fluorescence microscopy using a DeltaVision epifluorescence microscope as described (15).

Time-Lapse Microscopy. Cells were grown at 37 °C in C+Y medium and attached to thin 1.5% low-melting agarose C+Y matrix. The microscope slide was incubated at 30 °C in a temperature-controlled chamber of the DeltaVision microscope. Phase-contrast and fluorescence pictures were taken every 8 or 10 min, basically as described (15).

1. Martin B, García P, Castanié MP, Claverys JP (1995) The *recA* gene of *Streptococcus pneumoniae* is part of a competence-induced operon and controls lysogenic induction. *Mol Microbiol* 15:367–379.
2. Kloosterman TG, Bijlsma JJ, Kok J, Kuipers OP (2006) To have neighbour's fare: extending the molecular toolbox for *Streptococcus pneumoniae*. *Microbiology* 152:351–359.
3. Sambrook J (2001) *Molecular cloning: a laboratory manual* (Cold Spring Harbor Laboratory, Cold Spring Harbor, NY).
4. Eberhardt A, Wu LJ, Errington J, Vollmer W, Veening JW (2009) Cellular localization of choline-utilization proteins in *Streptococcus pneumoniae* using novel fluorescent reporter systems. *Mol Microbiol* 74:395–408.
5. Nováková L, et al. (2005) Characterization of a eukaryotic type serine/threonine protein kinase and protein phosphatase of *Streptococcus pneumoniae* and identification of kinase substrates. *FEBS J* 272:1243–1254.
6. Osaki M, et al. (2009) The StkP/PhpP signaling couple in *Streptococcus pneumoniae*: cellular organization and physiological characterization. *J Bacteriol* 191:4943–4950.
7. Fadda D, et al. (2007) *Streptococcus pneumoniae* DivIVA: localization and interactions in a MinCD-free context. *J Bacteriol* 189:1288–1298.
8. Canova MJ, Kremer L, Molle V (2008) pETPhos: a customized expression vector designed for further characterization of Ser/Thr/Tyr protein kinases and their substrates. *Plasmid* 60:149–153.
9. Claverys JP, Dintilhac A, Pestova EV, Martin B, Morrison DA (1995) Construction and evaluation of new drug-resistance cassettes for gene disruption mutagenesis in *Streptococcus pneumoniae*, using an ami test platform. *Gene* 164:123–128.
10. Minnen A, Attaiech L, Thon M, Gruber S, Veening JW (2011) SMC is recruited to *oriC* by ParB and promotes chromosome segregation in *Streptococcus pneumoniae*. *Mol Microbiol* 81:676–688.
11. Sliusarenko O, Heinritz J, Emonet T, Jacobs-Wagner C (2011) High-throughput, subpixel precision analysis of bacterial morphogenesis and intracellular spatio-temporal dynamics. *Mol Microbiol* 80:612–627.
12. Daniel RA, Errington J (2003) Control of cell morphogenesis in bacteria: two distinct ways to make a rod-shaped cell. *Cell* 113:767–776.
13. Albarracín Orio AG, Piñas GE, Cortes PR, Cian MB, Echenique J (2011) Compensatory evolution of pbp mutations restores the fitness cost imposed by β-lactam resistance in *Streptococcus pneumoniae*. *PLoS Pathog* 7:e1002000.
14. Pinho MG, Errington J (2003) Dispersed mode of *Staphylococcus aureus* cell wall synthesis in the absence of the division machinery. *Mol Microbiol* 50:871–881.
15. de Jong I, Beilharz K, Kuipers OP, Veening JW (2011) Live cell imaging of *Bacillus subtilis and Streptococcus pneumoniae* using automated time-lapse microscopy. *J Vis Exp* 28;(53):3145.

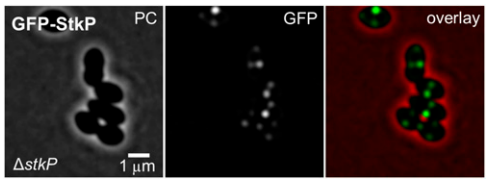

Fig. S1. Localization of GFP-StkP in a Δ*stkP* mutant. Micrographs of strains KB02-21 (P_{Zn}-*gfp-stkP*, Δ*stkP*). Exponentially growing cells in C+Y medium at 30 °C were harvested for fluorescence microscopy after 1 h of induction with 0.15 mM $ZnSO_4$. Phase contrast (PC), the GFP signal, and an overlay are shown. (Scale bar, 1 μm.)

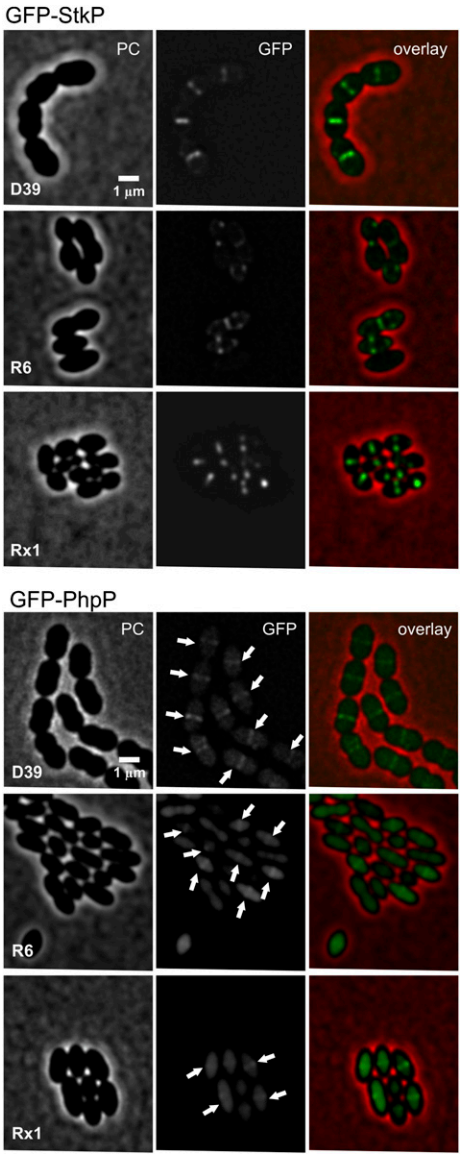

Fig. S2. Midcell localization of GFP-StkP and GFP-PhpP in D39, R6, and Rx1 genetic backgrounds. Micrographs of strains KB01-15 (P_{Zn}-*gfp-stkP*; D39), KB02-20 (P_{Zn}-*gfp-stkP*; R6), Sp32 (P_{Zn}-*gfp-stkP*; Rx1), KB01-14 (P_{Zn}-*gfp-phpP*; D39), KB02-23 (P_{Zn}-*gfp-phpP*; R6), and Sp31 (P_{Zn}-*gfp-phpP*; Rx1) are shown. Exponentially growing cells in C+Y medium at 37 °C were harvested for fluorescence microscopy after 1 h of induction with 0.15 mM $ZnCl_2$. Phase contrast (PC), the GFP signal, and an overlay are shown. Arrows indicate regions of enriched localization. (Scale bar, 1 μm.)

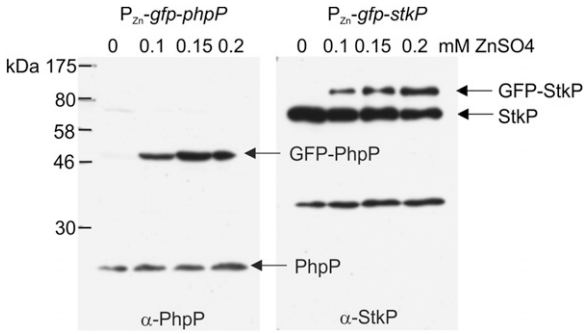

Fig. S3. StkP and PhpP expression. Expression of GFP-PhpP and GFP-StkP in a wild-type background. Strains were cultivated in GM17 medium until OD_{600} 0,2 and $ZnSO_4$ was added at concentrations indicated. Cells were harvested after 1 h, and protein lysates were separated by SDS/PAGE and immunoblotted with anti-PhpP or anti-StkP polyclonal antibody. GFP fusions and native PhpP and StkP are indicated by arrows.

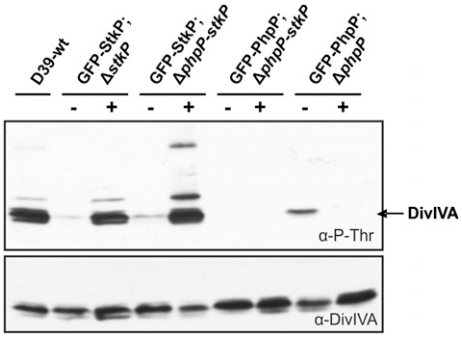

Fig. S4. The functionality of GFP-StkP and GFP-PhpP was confirmed by analyzing proteins phosphorylated in vivo. Phosphorylation of proteins on Thr residues was immunodetected using anti-pThr in total protein extracts of strains wild-type D39, KB01-18 (GFP-StkP; Δ*stkP*), KB01-20 (GFP-StkP; Δ*phpP-stkP*), KB01-21 (GFP-PhpP; Δ*phpP-stkP*), and KB01-19 (GFP-PhpP; Δ*phpP*). Expression of GFP-StkP or GFP-PhpP was induced (+) with 0.15 mM $ZnCl_2$ or was not induced (–). Immunodetection of DivIVA (α-DivIVA) in all samples served as a control. (*Upper*) Anti-pThr (α–P-Thr) immunodetection with antibody against phosphothreonine. (*Lower*) Anti-DivIVA, immunodetection with antibody against DivIVA. Note the hyperphosphorylation pattern in the absence of PhpP (strain KB01-20). Also note the reduced phosphorylation of DivIVA in the absence of PhpP (KB01-19 w/o zinc). This result can be explained in part by a likely polar effect on *stkP* gene expression in the *phpP* knockout.

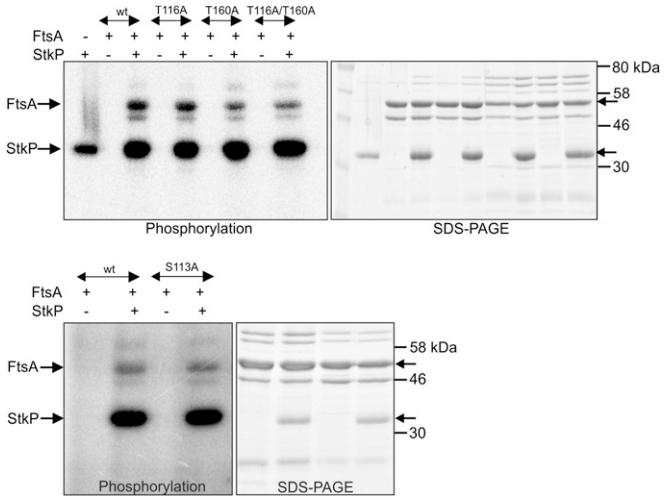

Fig. S5. In vitro phosphorylation of FtsA by StkP. Recombinant His-FtsA, His-FtsA-T116A, His-FtsA-T160A, His-FtsA-T116A/T160A, and His-FtsA-S113A were incubated with or without StkP-KD in kinase buffer in the presence of γ[^{32}P]ATP as described in *SI Materials and Methods*. Samples were separated by SDS/PAGE, and phosphorylation was detected by exposure of the Coomassie blue-stained gel to a sensitive screen.

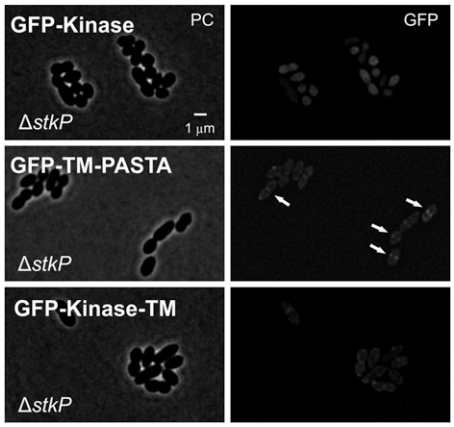

Fig. S6. Localization of StkP domains in a Δ*stkP* mutant. Micrographs of strains KB02-79 (P_{Zn}-*gfp-kinase*, Δ*stkP*), KB02-81 (P_{Zn}-*gfp-TM-PASTA*$_{1–4}$, Δ*stkP*), and KB02-80 (P_{Zn}-*gfp-kinase-TM*, Δ*stkP*). Exponentially growing cells in C+Y medium at 30 °C were harvested for fluorescence microscopy after 1 h of induction with 0.15 mM $ZnSO_4$. Phase contrast (PC) and the GFP signal are shown. Arrows indicate regions of enriched localization. (Scale bar, 1 μm.)

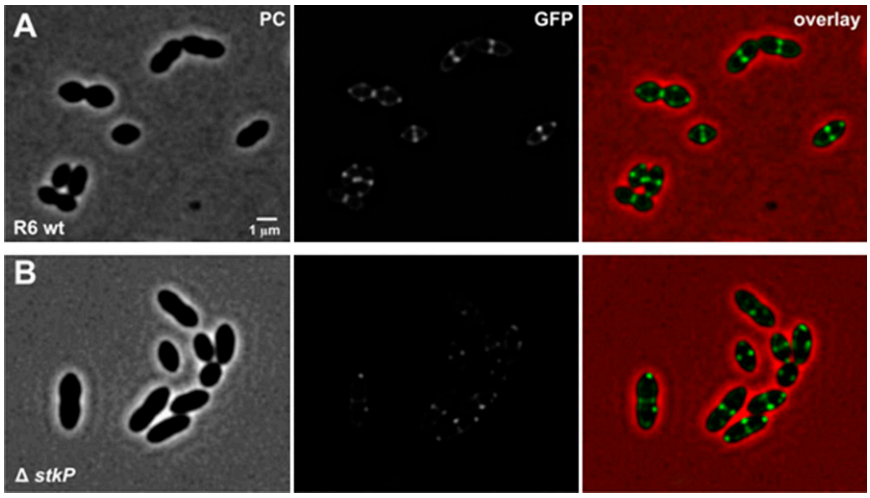

Fig. S7. Localization of GFP-StkP-K42R. Micrographs of strains (*A*) KB02-77 (P_{Zn}-*gfp-stkP-K42R*) and (*B*) KB02-78 (P_{Zn}-*gfp-stkP-K42R*, Δ*stkP*). Exponentially growing cells in C+Y medium at 37 °C were harvested for fluorescence microscopy after 1 h of induction with 0.15 mM $ZnSO_4$. Phase contrast (PC), the GFP signal, and an overlay are shown. (Scale bar, 1 μm.)

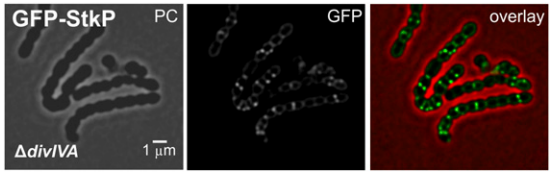

Fig. S8. Localization of GFP-StkP in Δ*divIVA*. Micrographs of strain KB02-34 (P_{Zn}-*gfp-stkP*, Δ*divIVA*). Exponentially growing cells in C+Y medium at 37 °C were harvested for fluorescence microscopy after 1 h of induction with 0.15 mM $ZnSO_4$. Phase contrast (PC), the GFP signal, and an overlay are shown. (Scale bar, 1 μm.)

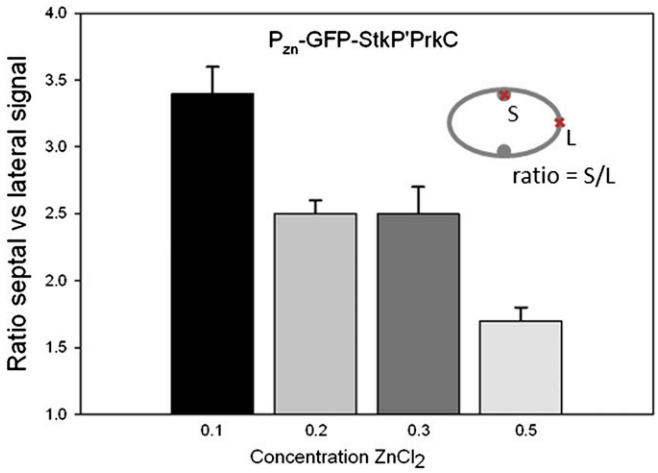

Fig. S9. Midcell vs. lateral localization of P_{Zn}-GFP-PrkC′-StkP′ with increasing induction levels. Septal (midcell) (S) and lateral (L) membrane fluorescence of strain KB02-59 (R6; PZn-GFP-StkP'PrkC) was quantified at five separate points per individual cell, and the ratio of septal fluorescence signal to lateral signal was determined and compared for induction with different concentrations of $ZnCl_2$ (0.1, 0.2, 0.3, and 0.5 mM). The ratios of ~50 cells per sample were calculated as in ref. 1. Error bars represent SEM.

1. Atilano ML, et al. (2010) Teichoic acids are temporal and spatial regulators of peptidoglycan cross-linking in *Staphylococcus aureus*. *Proc Natl Acad Sci USA* 107:18991–18996.

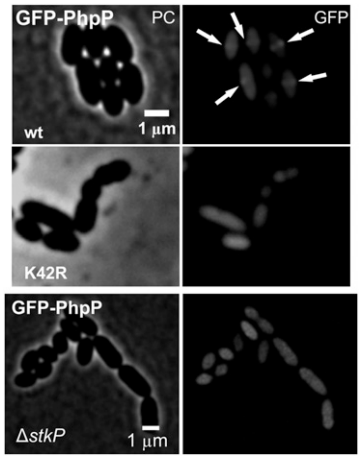

Fig. S10. Loss of midcell localization of GFP-PhpP in a Δ*stkP* and in a *stkP-K42R* genetic background. Micrographs of strains Sp31 (P_{Zn}-*gfp-phpP*, Rx1), Sp79 (P_{Zn}-*gfp-phpP*, *stkPK42R,* Rx1), and KB02-66 (P_{Zn}-*gfp-phpP*, Δ*stkP*, R6). Exponentially growing cells (OD_{600} nm 0.2) in C+Y medium at 37 °C were harvested for fluorescence microscopy after 1 h of induction with 0.15 mM $ZnSO_4$. Phase contrast (PC) and the GFP signal are shown. Arrows indicate midcell localization of GFP-PhpP. (Scale bar, 1 μm.)

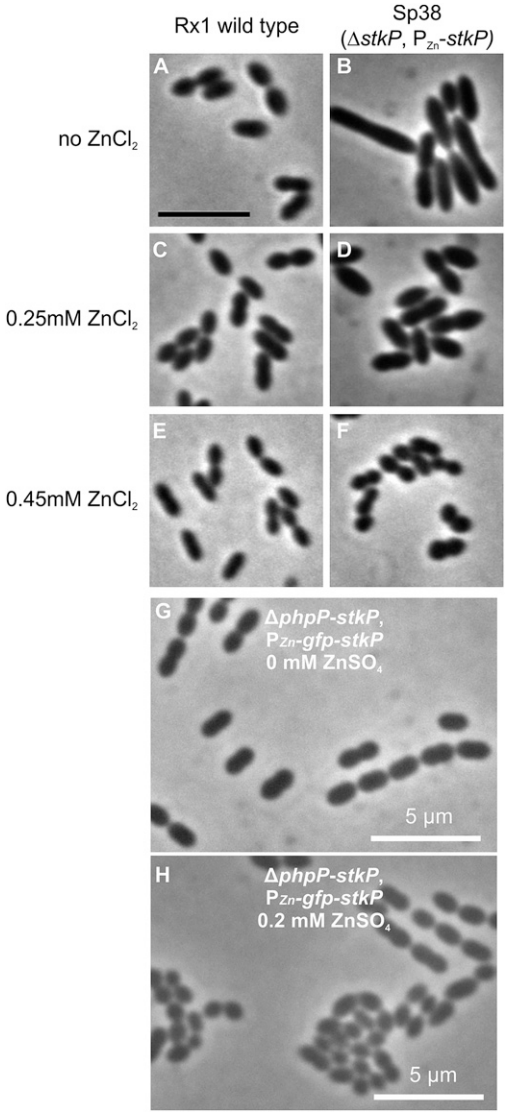

Fig. S11. Complementation of Δ*stkP*. Phase-contrast microscopy of *S. pneumoniae* wild-type Rx1 and complementation strain Sp38 carrying a copy of the *stkP* gene under the zinc-inducible promoter (Δ*stkP*, *bgaA*::P_{Zn}-*stkP*). Strains were grown on Columbia blood agar plates with or without $ZnCl_2$ at 37 °C. Cells were harvested after 6 h of growth and examined with an Olympus BX-60 microscope equipped with a phase-contrast oil immersion objective (100×). (*A*) Wild-type Rx1. (*B*) Sp38. (*C*) Rx1 with 0.25 mM $ZnCl_2$. (*D*) Sp38 with 0.25 mM $ZnCl_2$. (*E*) Rx1 with 0.45 mM $ZnCl_2$. (*F*) Sp38 with 0.45 mM $ZnCl_2$. (Scale bar, 5 μm.) (*G* and *H*) Phase-contrast micrographs show *S. pneumoniae* D39 wild-type strain (*G*) and strain KB01-20 (Δ*phpP-stkP*, *bgaA*::P_{Zn}-*gfp-stkP*) (*H*) induced with 0.2 mM $ZnSO_4$ at 37 °C. Cells were harvested at OD_{600} 0.25. (Scale bar, 5 μm.)

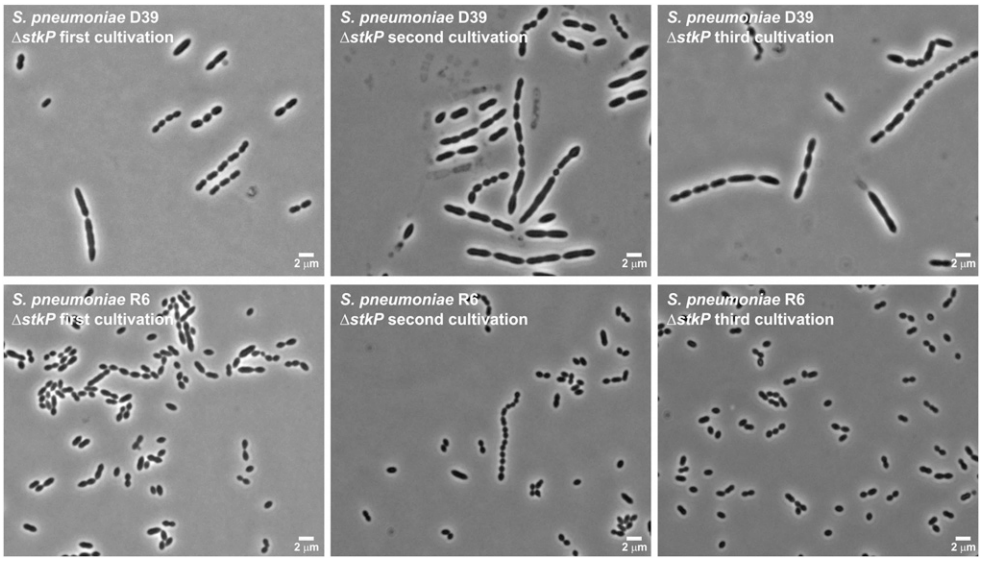

Fig. S12. Appearance of Δ*stkP* suppressor mutations. Single colonies of a fresh transformation generating Δ*stkP* cells using pDELstkP DNA were grown in C+Y medium and examined by phase-contrast microscopy at midexponential growth (OD_{600} ~0.2). A single colony of the transformation plate was resuspended in C+Y medium, and a dilution series was plated to generate single colonies within Colombia blood agar. The next day, subsequent single colonies (T2 plate) were grown in liquid C+Y medium and examined as before (second cultivation). A single colony from the T2 plate was replated as before, and cells were grown and examined as described above (third cultivation). Although the typical elongated-cell phenotype for Δ*stkP* mutants remained the same after cultivation in the D39 genetic background, the elongated phenotype was lost rapidly in the R6 genetic background, and a pleiotropic array of cell morphologies was observed. After the second cultivation many chains of cells can be observed, but after the third cultivation small, round cells were observed. The genetic differences between D39 and R6, especially in important cell division proteins, might account for the more rapid appearance of Δ*stkP* suppressors in the R6 genetic background (1).

1. Lanie JA, et al. (2007) Genome sequence of Avery's virulent serotype 2 strain D39 of *Streptococcus pneumoniae* and comparison with that of unencapsulated laboratory strain R6. *J Bacteriol* 189:38–51.

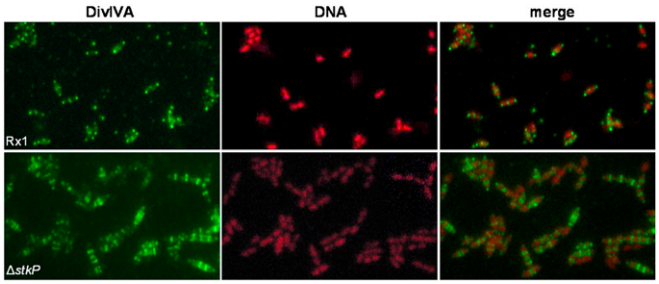

Fig. S13. Perturbed assembly of DivIVA in the absence of StkP. DivIVA subcellular localization in wild-type Rx1 cells and in Rx1 cells in which StkP is depleted (strain Sp38; *ΔstkP*, P_{Zn}-*stkP*) as detected by immunofluorescence using anti-DivIVA polyclonal antibodies. Cells were stained to visualize DivIVA (green) and DNA (red); the merged images show the localization of DivIVA and DNA simultaneously.

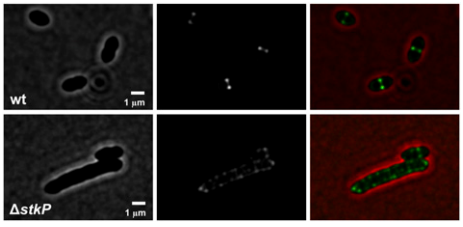

Fig. S14. Unbalanced cell-wall synthesis in the absence of StkP. Van-FL staining of wild-type R6 cells and in cells mutated for *stkP*. Cells were grown in C+Y medium. Van-FL and unlabeled vancomycin were added in a 1:1 ratio (final concentration, 0.2 μg/mL) to midexponentially growing cells, and cells were incubated on ice for 5 min before imaging with fluorescence microscopy, conducted essentially as described (1). This analysis also shows perturbed cell-wall synthesis with significantly more signal at the periphery of the cells in the Δ*stkP* mutant. Note that cells in Fig. 7*B* were depleted for StkP using the zinc-inducible system, and samples were fixed using formaldehyde before imaging. The two experimental procedures generate the same conclusion.

1. Daniel RA, Errington J (2003) Control of cell morphogenesis in bacteria: two distinct ways to make a rod-shaped cell. *Cell* 113:767–776.

Table S1. Plasmids and bacterial strains used in this study

Strain/plasmid	Relevant genotype	Reference
S. pneumoniae		
D39	Serotype 2 strain	(1)
R6	D39 (Δ*cps2* 2538–9862), nonencapsulated	(2)
Rx1	Nonencapsulated strain	(3)
Sp10	Rx1, *cm*, Δ*stkP*::*cm*	(4)
HK95	R6, *tet*, *bgaA*::P_{Zn}-*gfp-ftsA*, P_{Zn}-*rfp-stkP*	This study
HK96	R6, *tet*, *bgaA*::P_{Zn}-*divIVA-gfp*, P_{Zn}-*rfp-stkP*	This study
JWV403	D39, *tet*, *bgaA*::P_{Zn}-*gfp-kinase*	This study
KB01-14	D39, *tet*, *bgaA*::P_{Zn}-*gfp-phpP*	This study
KB01-15	D39, *tet*, *bgaA*::P_{Zn}-*gfp-stkP*	This study
KB01-16	D39, *tet*, *bgaA*::P_{Zn}-*gfp-TM-PASTA*	This study
KB01-18	D39, *cm*, *tet*, Δ*stkP*::*cm*, *bgaA*::P_{Zn}-*gfp-stkP*	This study
KB01-19	D39, *cm*, *tet*, Δ*phpP*::*cm*, *bgaA*::P_{Zn}-*gfp-phpP*	This study
KB01-20	D39, *cm*, *tet*, Δ*phpP-stkP*::*cm*, *bgaA*::P_{Zn}-*gfp-stkP*	This study
KB01-21	D39, *cm*, *tet*, Δ*phpP-stkP*::*cm*, *bgaA*::P_{Zn}-*gfp-phpP*	This study
KB01-40	D39, *tet*, *bgaA*::P_{Zn}-*gfp-TM-kinase*	This study
KB02-20	R6, *tet*, *bgaA*::P_{Zn}-*gfp-stkP*	This study
KB02-21	R6, *cm*, *tet*, Δ*stkP*::*cm*, *bgaA*::P_{Zn}-*gfp-stkP*	
KB02-22	R6, *cm*, Δ*phpP-stkP*::*cm*, *bgaA*::P_{Zn}-*gfp-stkP*	This study
KB02-23	R6, *tet*, *bgaA*::P_{Zn}-*gfp-phpP*	This study
KB02-29	R6, *cm*, Δ*stkP*::*cm*	This study
Rx1-Δ*divIVA*	Rx1, Δ*divIVA*::*cm*	(5)
KB02-34	R6, *tet*, *bgaA*::P_{Zn}-*gfp-stkP;* Δ*divIVA*::*cm*	This study
KB02-59	R6, *tet*, *bgaA*::P_{Zn}-*gfp-stkP′-prkC*	This study
KB02-61	R6, *tet*, *cm*, Δ*stkP*::*cm*, *bgaA*::P_{Zn}-*gfp-stkP′-prkC′*	This study
KB02-62	R6, *tet*, *bgaA*::P_{Zn}-*gfp-ftsA*	This study
KB02-63	R6, *tet*, *bgaA*::P_{Zn}-*divIVA-gfp*	This study
KB02-64	R6, *cm*, *tet*, Δ*stkP*::*cm*, *bgaA*::P_{Zn}-*divIVA-gfp*	This study
KB02-65	R6, *cm*, *tet*, Δ*stkP*::*cm*, *bgaA*::P_{Zn}-*gfp-ftsA*	This study
KB02-66	R6, *cm*, *tet*, Δ*stkP*::*cm*, *bgaA*::P_{Zn}-*gfp-phpP*	This study
KB02-26	R6, *tet*, *bgaA*::P_{Zn}-*gfp-kinase*	This study
KB02-27	R6, *tet*, *bgaA*::P_{Zn}-*gfp-TM-PASTA*	This study
KB02-28	R6, *tet*, *bgaA*::P_{Zn}-*gfp-TM-kinase*	This study
KB02-77	R6, *tet*, *bgaA*::P_{Zn}-*gfp-StkP-K42R*	This study
KB02-78	R6, *tet*, *bgaA*::P_{Zn}-*gfp-StkP-K42R;* Δ*stkP*::*cm*	This study
KB02-79	R6, *tet*, *bgaA*::P_{Zn}-*gfp-kinase*, Δ*stkP*	This study
KB02-81	R6, *tet*, *bgaA*::P_{Zn}-*gfp-TM-PASTA*, Δ*stkP*	This study
KB02-80	R6, *tet*, *bgaA*::P_{Zn}-*gfp-TM-kinase*, Δ*stkP*	This study
Sp31	Rx1, *tet*, *bga*::P_{Zn}-*gfp-phpP*	This study
Sp32	Rx1, *tet*, *bgaA*::P_{Zn}-*gfp-stkP*	This study
Sp38	Rx1, *tet*, *bgaA*::P_{Zn}-*stkP*, Δ*stkP*	This study
Sp79	Rx1, *tet*, *bga*::P_{Zn}-*gfp-phpP, stkP-K42R*	This study
E. coli		
EC1000	F^-, *araD139* (*ara ABC-leu*)*7679*, *galU*, *galK*, *lacX74*, *rspL*, *thi*, *repA* of pWV01 in *glgB*, *km*	(6)
BL21	F^-, *dcm*, *ompT*, *hsdS*(r_B- m_B-), *gal*, $[malB^+]_{K\text{-}12}(\lambda^S)$	Stratagene
Plasmids		
pBluescript II KS^-	*Amp*	Stratagene
pJWV25	*Amp*, *tet*, *bgaA*, P_{Zn}-*gfp*+	(7)
pEVP3	*cm*	(8)
pDELstkP	*Cm, amp, stkP-flanking regions*	(4)
pETPhos	*Amp*	(9)
pEX-StkP-T	*Amp, IPTG-inducible StkP-kinase domain*	(4)
pEX-StkP-K42R	*Amp, IPTG-inducible StkP-K42R*	(4)
pDELphpP	*Cm, amp, phpP-flanking regions*	This study
pDELphpP-stkP	*Cm, amp, phpP-stkP- flanking regions*	This study
pETPhos-1511	*Amp, ftsA*	This study
pETPhos-1511-T116A	*Amp, ftsA-T116A*	This study
pETPhos-1511-T160A	*Amp, ftsA-T160A*	This study
pETPhos-1511-T116A/T160A	*Amp, ftsA-T116A/T160A*	This study
pETPhos-1511-S113A	*Amp, ftsA-S113A*	This study
pZn-StkP	*Amp*, *tet*, *bgaA*, P_{Zn}-*stkP*	This study
pJWV25-stkP	*Amp*, *tet*, *bgaA*, P_{Zn}-*gfp-stkP*	This study

Table S1. Cont.

Strain/plasmid	Relevant genotype	Reference
pJWV25-phpP	*Amp*, *tet*, *bgaA*, P_{Zn}-*gfp-phpP*	This study
pJWV25-kinase	*Amp*, *tet*, *bgaA*, P_{Zn}-*gfp-kinase*	This study
pJWV25-TM-kinase	*Amp*, *tet*, *bgaA*, P_{Zn}-*gfp-TM-kinase*	This study
pJWV25-PASTA	*Amp*, *tet*, *bgaA*, P_{Zn}-*gfp-PASTA*	This study
pJWV25-stkP′-prkC′	*Amp*, *tet*, *bgaA*, P_{Zn}-*gfp-stkP′-prkC′*	This study
pJWV25-DivIVA-GFP	*Amp*, *tet*, *bgaA*, P_{Zn}-*divIVA-gfp*	This study
pJWV25-gfp-ftsA	*Amp*, *tet*, *bgaA*, P_{Zn}-*gfp-ftsA*	This study

Amp; ampicillin resistance marker; *cm*; chloramphenicol resistance marker; IPTG, isopropyl thio-β-D-galactoside; *km*; kanamycin resistance marker; *tet*; tetracycline resistance marker.

1. Avery OT, Macleod CM, McCarty M (1944) Studies on the chemical nature of the substance inducing transformation of pneumococcal types. Induction of transformation by a desoxyribonucleic acid fraction isolated from Pneumococcus type III. *J Exp Med* 79:137–158.
2. Hoskins J, et al. (2001) Genome of the bacterium *Streptococcus pneumoniae* strain R6. *J Bacteriol* 183:5709–5717.
3. Ravin AW (1959) Reciprocal capsular transformations of pneumococci. *J Bacteriol* 77:296–309.
4. Nováková L, et al. (2005) Characterization of a eukaryotic type serine/threonine protein kinase and protein phosphatase of *Streptococcus pneumoniae* and identification of kinase substrates. *FEBS J* 272:1243–1254.
5. Fadda D, et al. (2007) *Streptococcus pneumoniae* DivIVA: Localization and interactions in a MinCD-free context. *J Bacteriol* 189:1288–1298.
6. Leenhouts K, et al. (1996) A general system for generating unlabelled gene replacements in bacterial chromosomes. *Mol Gen Genet* 253:217–224.
7. Eberhardt A, Wu LJ, Errington J, Vollmer W, Veening JW (2009) Cellular localization of choline-utilization proteins in *Streptococcus pneumoniae* using novel fluorescent reporter systems. *Mol Microbiol* 74:395–408.
8. Claverys JP, Dintilhac A, Pestova EV, Martin B, Morrison DA (1995) Construction and evaluation of new drug-resistance cassettes for gene disruption mutagenesis in *Streptococcus pneumoniae*, using an ami test platform. *Gene* 164:123–128.
9. Canova MJ, Kremer L, Molle V (2008) pETPhos: a customized expression vector designed for further characterization of Ser/Thr/Tyr protein kinases and their substrates. *Plasmid* 60: 149–153.

Table S2. Oligonucleotides

Primer	Sequence (5′ to 3′)	Restriction site
CAT1	CGCGGATCCGAAAATTTGTTTGATTTTTAA	BamHI
CAT2	GCTCTAGAGGGTTCCGACCGTCAACGTCAA	XbaI
CAT3	GCTCTAGAAAGTACAGTCGGCATTAT	XbaI
DFKFP	GCTCTAGAATCTACAAACCTAAAACAAC	XbaI
DFKRP	TGCCCGCGGTCATAATATCACGGACCGCAT	SacII
ftsA-F+SpeI	GCGCACTAGTGCTAGAGAAGGCTTTTTTACAGG	SpeI
ftsA-R+NotI	CGAAGCGGCCGCCTCCTCTTTATTCGTCAAACATGCTTCC	NotI
LN120	CTTGCCGATTTGGATAAGATGTTTCATATTTGCCTCCT	
LN121	AATATGAAACATCTTATCCAAATCGGCAAGATTTT	
LN123	TTCGCTACTTGGAGCCACTAT	
LN131	AAGGAGGCAAATATGCCAATTACATCATTAGAAATAAA	
LN133	TAATGATGTAATTGGCATATTTGCCTCCTTAAGATCC	
LN134	ATTAGCGGCCGCTTAAGGAGTAGCTGAAGTTGTTTT	
LN144	TGGAACTAGTATCCAAATCG	SpeI
LN145	TTTGACATCCTTAGGAGTTCTGGATAGTATCCAAAT	
LN146	ATACTATCCAGAACTCCTAAGGATGTCAAAATACCT	
LN147	CGGCGCGGCCGCTTATTCATCTTTCGGATACTC	NotI
LN179	ATGAAGAACCAGAAGTCTAGAGGATCTGGTGGAGAAGCTGCAGCTA AAGCTGGAACTAGTATCAGCAAAGGAGAAGAACTTTTC	
LN180	ATTAGCGGCCGCTTATTTGTAGAGCTCATCCATG	NotI
LN181	accagatcctctagaCTTCTGGTTCTTCATACA	
LN182	CGGCCATATGGCTAGAGAAGGCTTTTTT	NdeI
LN183	GCCGCTCGAGTTATTCGTCAAACATGCTTCC	XhoI
LN186	ATGTTGTCAAATCAGCTTTGGCAAAGAGTATGACACCTGAC	
LN187	GTCAGGTGTCATACTCTTTGCCAAAGCTGATTTGACAACAT	
LN188	CTTGAAATGCGTGGTTTGCTTTATGCAGGACCTCGTAC	
LN189	GTACGAGGTCCTGCATAAAGCAAACCACGCATTTCAAG	
LN190	CAAGATGTTGAAAATGTTGTCAAAGCAGCTTTGACAAAGAGTATGAC	
LN191	GTCATACTCTTTGTCAAAGCTGCTTTGACAACATTTTCAACATCTTG	
phpP-F+SpeI	CGCGACTAGTGAAATTTCATTATTAACAGATG	SpeI
phpP-R+NotI	CGAAGCGGCCGCTTATCATTCTGCATCCTCCTCGTTCATAGAAAC	NotI
stkP-F+SpeI	CGCGACTAGTATCCAAATCGGCAAGATTTTTGCCGG	SpeI
stkP-kinase-R+NotI	CGAAGCGGCCGCTTATTGGTAAGTTTCCTCTGTCACAGC	NotI
stkP-PASTA-F+SpeI	CGCGACTAGTTTGGCCAGCCTTGTATTGGTGGCAGC	SpeI
stkP-R+NotI	CGAAGCGGCCGCTTAAGGAGTAGCTGAAGTTGTTTTAGGTTTGTAG	NotI
StkP-TM-R NotI	CGAAGCGGCCGCTTAGGCAATGGTTGCAGGAGTTCTGGATAG	NotI
UFPFP	CGCGAATTCTGGTTGCTCCGACGCTTGATT	EcoRI
UFPRP	CGCGGATCCTAATAATGAAATTTCCATGT	BamHI

Relevant restriction sites are underlined.

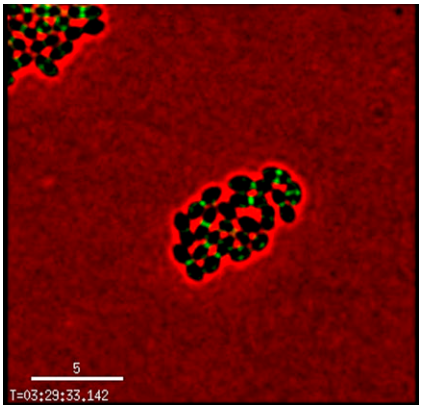

Movie S1. Time-lapse analysis of strain KB02-20 (P_{Zn}-*gfp-stkP*). The movie is comprised of an overlay of GFP (green) and phase-contrast (red) images. (Scale bar, 5 μm.)

Movie S1

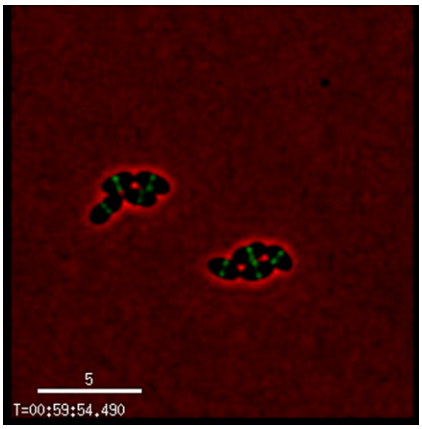

Movie S2. Time-lapse analysis of strain KB02-26 (P_{Zn}-*gfp-ftsA*). The movie is comprised of an overlay of GFP (green) and phase-contrast (red) images. (Scale bar, 5 μm.)

Movie S2

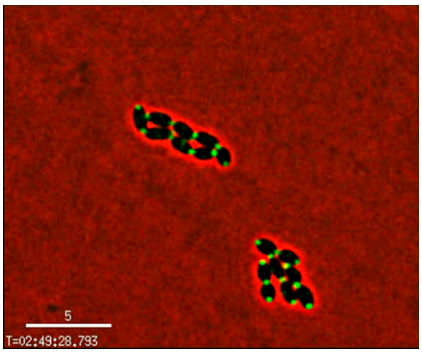

Movie S3. Time-lapse analysis of strain KB02-63 (P_{Zn}-*divIVA-gfp*). The movie is comprised of an overlay of GFP (green) and phase-contrast (red) images. (Scale bar, 5 μm.)

Movie S3

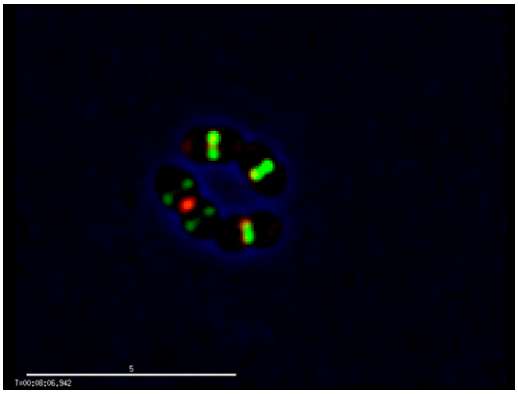

Movie S4. Time-lapse analysis of strain HK95 (P_{Zn}-*gfp-ftsA*, P_{Zn}-*rfp-stkP*). The movie is comprised of an overlay of phase-contrast (blue), GFP (green) and RFP (red) images. (Scale bar, 5 μm.)

Movie S4

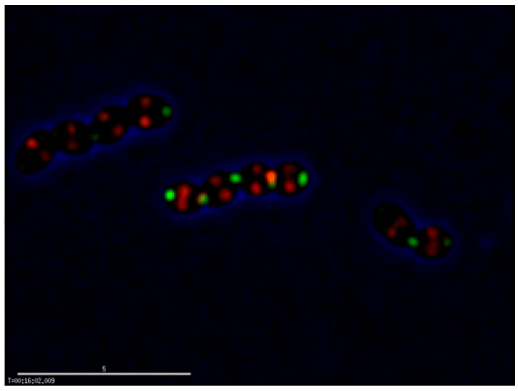

Movie S5. Time-lapse analysis of strain HK96 (P_{Zn}-*divIVA-gfp*, P_{Zn}-*rfp-stkP*). The movie is comprised of an overlay of phase-contrast (blue), GFP (green) and RFP (red) images. (Scale bar, 5 μm.)

Movie S5

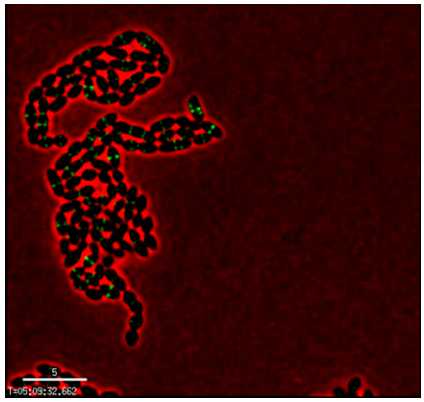

Movie S6. Time-lapse analysis of strain KB02-65 (P_{Zn}-*gfp-ftsA*, Δ*stkP*). The movie is comprised of an overlay of GFP (green) and phase-contrast (red) images. (Scale bar, 5 μm.)

Movie S6

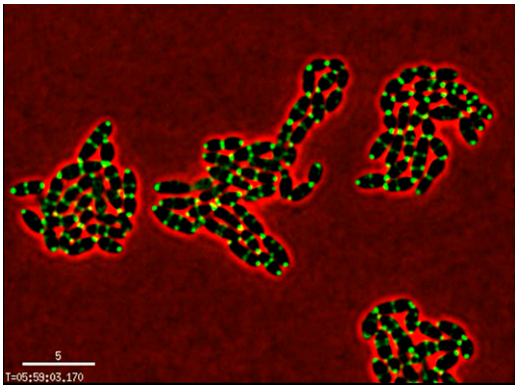

Movie S7. Time-lapse analysis of strain KB02-65 (P_{Zn}-*divIVA-gfp*, Δ*stkP*). The movie is comprised of an overlay of GFP (green) and phase-contrast (red) images. (Scale bar, 5 μm.)

Movie S7